Utilizing Dynamic Fuel Pressure Sensor For Detecting Bearing Spalling and Gear Pump Failure Modes in Cummins Pressure Time (PT) Pumps

J. Scott Pflumm, Jeffrey C. Banks

Applied Research Laboratory, State College, PA, 16801, USA

jsp116@arl.psu.edu
jcb242@arl.psu.edu

ABSTRACT

The objective of this paper is to highlight the results of the fault detection investigation conducted to ascertain the feasibility of exploiting the existing on-board M2/M3 Bradley fuel pressure sensor for the purpose of detecting mechanical bearing spalling and gear pump failure modes of the pressure-time (PT) fuel pump used on the Cummins VTA-903T engine. To investigate this fluid-mechanical cross domain detection approach, a Bradley fuel system test bed was built. Fault tests for four PT pump failure modes were conducted including bearing faults, gear pump fault, idle adjust mis-calibration, and air-fuel control fault. The results of the first two fault tests are summarized in this paper. Due to limited number of pumps available for testing (2), these preliminary findings are not statistically substantiated. With this stated, the findings present a method for investigating the presence of a narrowband frequency-domain-based predictive fault detection capability using the existing pressure sensor installed on the Chassis Modernization and Embedded Diagnostics (CMED) variant Bradley. The test stand based seeded fault analysis was not capable of detecting an 0.080 inch outer raceway bearing spall, but there is preliminary evidence to warrant further study that a nominal 0.001 inch foreign object debris accumulation on the gear teeth of the gear pump might be detectable using a simple kurtosis based calculation using a pressure sensor with a 0-500 Hz dynamic bandwidth.

1. INTRODUCTION

The Program Management Office for the Heavy Brigade Combat Team (PM-HBCT) is leading the development of a Vehicle Health Management System (VHMS) that provides the US Army with an improved diagnostic, predictive and sustainment capability for HBCT platforms including the M2/M3 Bradley Fighting Vehicle. The common challenge faced by the Program Management Office when evaluating VHMS technology is the requirement to install additional instrumentation or to modify the chassis of an existing fleet of vehicles. These requirements often detrimentally impact the cost-benefit decision to implement VHMS technology. This paper discusses utilizing a dynamic fuel pressure sensor existing on the CMED configuration of the M2/M3 Bradley in order to detect mechanical faults in the PT pump. The objective is to employ existing on-board sensors to extend the vehicle's present VHMS capability. Prior to this investigation a vehicle degrader analysis was conducted in order to ascertain where health monitoring technology would provide the greatest benefit in terms of decreasing diagnosis time, increasing maintenance effectiveness, decreasing No Evidence of Failure (NEOF) rates and facilitating the migration to a 2-tier maintenance system.

2. DEGRADER ANALYSIS

A Reliability Centered Maintenance (RCM) degrader analysis for the M2/M3 Bradley was conducted by the HBCT VHMS program to assess the top degraders of the vehicle's maintainability, reliability and operational availability (Banks, Reichard, Hines, Brought, 2008). The formal RCM process typically consists of regular meetings with subject matter experts (i.e. maintainers, design engineers, logisticians, CBM experts, etc.) to evaluate a system over a significant period of time (i.e. weeks to months). The length of time required for the analysis is dependent upon the complexity of the system and the knowledge level of the subject matter experts participating in the process. It was logistically prohibitive to regularly gather the subject matter experts required to conduct a formal RCM analysis for the U.S. Army's Bradley vehicle. Penn State ARL conducted a modified RCM analysis using the results of the degrader interviews, degrader OEM questionnaire, field service representative reports, technical manuals and engineering judgment. This process provides a systematic approach for the evaluation of the VHMS design,

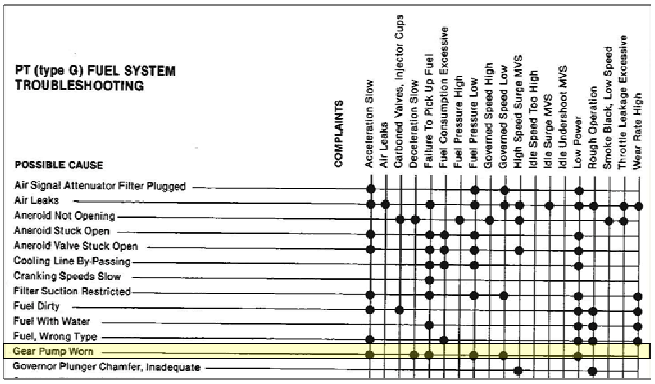

Figure 1. Troubleshooting cause-effect matrix excerpt from Cummins PT Fuel Pump Rebuilding and Calibration Instructions

functional requirements, failure modes and criticality assessment. From this assessment the appropriate and most effective maintenance approaches can be selected for the platform or system based on the operating context of the asset. The specific advantage of utilizing the RCM process when designing an asset health management system is the ability to determine where the implementation of embedded diagnostic technology would provide the greatest benefit in terms of facilitating improved maintainability and increased operational availability of the asset.

The degrader analysis reviewed Field Service Reports for the following 7 Bradley subsystems: Track and Suspension, Gun System, Electrical System, Turret Drive Control Unit, Transmission, Cable and Wiring, and Fuel System. A total of 769 failures were tallied across all subsystems. Four percent (4%) of all 769 failures involved the fuel system. Two percent (2%) of the 769 failures cited the PT pump as the failure mode. Approximately 50% of the 31 cited fuel system related failures involved the PT pump (Banks, Reichard, Hines Brought, 2008). Given the existence of a dynamic fuel pressure sensor located between the PT pump and fuel injectors, and the results of the degrader analysis, the Bradley fuel system was considered a candidate for investigating implementation of VHMS technology. The on-board dynamic fuel pressure sensor is not necessarily capable of detecting all the possible PT pump faults listed in figure 1. The underlying intent of utilizing the existing pressure sensor to support real-time on-board diagnostic capability is to investigate the greatest extent to which the sensor can be exploited to aid the operator/maintainer in terms of alerting the crew of impending fuel system faults, or automatically diagnosing a subcomponent fault that would not be apparent during routine preventive maintenance checks and services.

3. VEHICLE FUEL SYSTEM DESCRIPTION

The Bradley fuel system supports a Cummins VTA-903T water-cooled, eight cylinder diesel engine that rates 600 HP. The fuel system consists of two fuel tanks (upper and lower), four in-tank fuel pumps, a fuel/water separator, and a PT fuel pump/governor with integrated air-fuel control (AFC) valve.

In general, the fuel flows from the lower tank through two check valves and a main shut-off valve, through the filter/water separator to the PT pump/governor, which sends regulated high pressure fuel to the injectors as shown in figure 2 (Technical Manual, 2006). Control of engine power output and idle speed is accomplished by the engine mounted PT fuel pump/governor with integrated AFC valve. The fuel pressure to the injectors is regulated to between 129 psi - 163 psi depending on the pump version used with the electronic fuel control valve (EFCV). Excess fuel is returned to the tank through a low pressure return line.

The CMED equipped vehicles have a pressure transducer integrated into the fuel system. This sensor has a 0-500 Hz measurement capability and is located at the existing Bradley Standard Test Equipment – Internal Combustion Engine diagnostic test kit (BRADS-ICE) pressure sensor port. The CMED system monitors this pressure transducer during diagnostic/maintenance mode (the vehicle is not operational in this mode) and provides an indication of pump failure based on an insufficient pressure level while the engine is run at a high RPM condition. The limitation is that the AFC valve needs to be manually opened to conduct this procedure. This test can only be conducted when the platform is down for maintenance inspection.

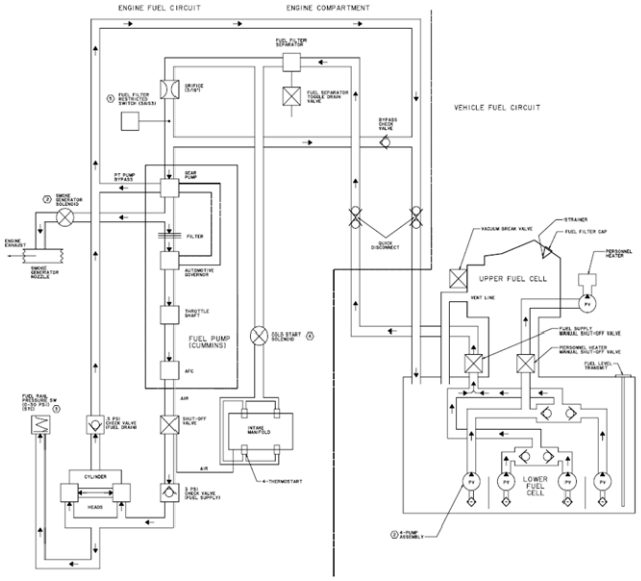

Figure 2. Bradley Fuel System Schematic

(TM 9-2350-294-20-1-1/3, 2000)

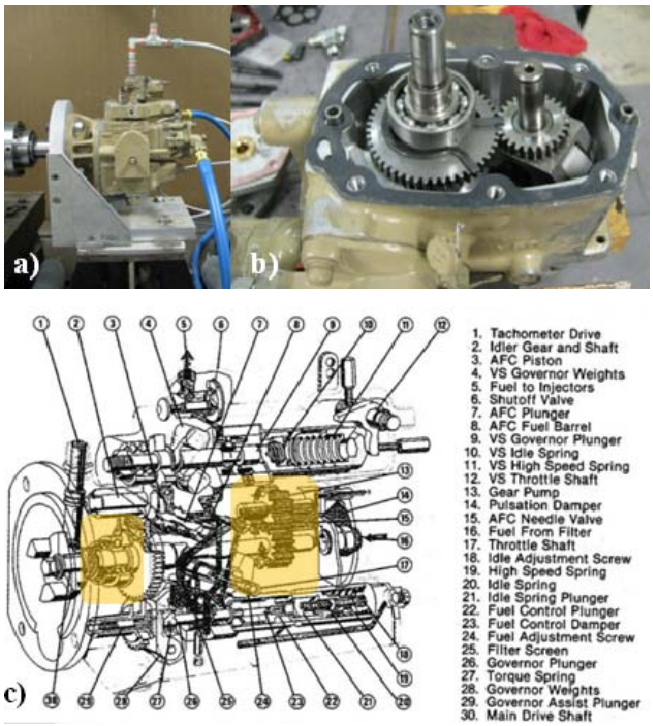

Figure 3. a) PT pump assembled; b) Partial disassembled; c) Schematic

Figure 3 shows three images depicting the PT pump. The bottom image is a schematic of a similar model PT pump, however it shows the relevant components most clearly. The yellow boxes highlight the subcomponents investigated in this analysis. The left-most yellow box highlights the front bearing. The right box highlights the gear pump gears.

4. TEST BED, SENSORS AND DATA ACQUISITION

The test bed consists of one fuel tank (representative of the lower tank), four in-tank fuel pumps, a fuel filter separator, and a PT fuel pump/governor with integrated air-fuel control (AFC) valve. The in-tank pumps, fuel filter separator, PT pump and commercial equivalent of the pressure transducer are configured in the same sequence as they are on the vehicle. On the test bed, fuel enters the in-tank fuel pump and continues through the fuel filter separator to the PT pump which is directly driven by a 30 HP AC electric motor. For simplicity in this phase of the project, the PT pump output, which is intended to supply fuel to the fuel injectors, is routed to a manual adjusted needle valve. The needle valve outlet pressure was set to nominal 160 PSIG and the air supply to the AFC check valve was set to 30 PSIG in accordance with Cummins Calibration Instruction Manuals (Cummins Bulletin Nrs. 3379352-10 and 3379084-02, 1980 and TM 9-2350-294-20-1-3). Validation data is maintained and available for review. The PT pump leakage and fuel supplied to the needle valve are returned directly into the sump tank to form a continuous closed loop non-combusting fuel circuit as shown in figure 4. For fault induction and component isolation purposes, the valves, flow meters, pressure transducers and thermocouples are located at the following locations:

- After the in-tank fuel pump and before the fuel filter separator
- After the fuel filter separator and before the PT pump
- After the PT pump and before the needle valve

A 16 channel National Instruments PXI based data acquisition system with 100 kSamples/second per channel capability is used to support data gathering. This data acquisition system collects user-triggered 10 second snapshots of the voltage and current sensors for monitoring the in-tank pump power, ICP tri-axial accelerometer mounted on the PT pump, fluid pressure and flow at each of the aforementioned three locations in the fluid circuit, as well as a torque cell measuring both torque and speed of the drive shaft to the PT pump.

The analysis emphasizes the findings of the pressure sensor in terms of its capability as an embedded diagnostic tool. The commercial version of this pressure sensor, which we used, provides higher bandwidth and is therefore capable of higher resolution data processing techniques that are otherwise not available with the existing on-board 0-500 Hz pressure sensor. Our goal is to limit our analysis to what is implementable given the operational bandwidth of this 0-500 Hz on-board pressure transducer.

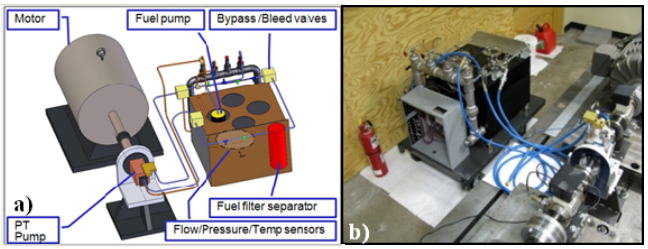

Figure 4. a) Drawing Bradley Fuel System Test Bed b) Photo

5. TESTING OVERVIEW

The test approach can be summarized briefly as follows: first investigate failure modes that do not result in permanent damage to the pump, then progress deeper into failure modes that permanently damage the pump or its subcomponents. The rationale for this approach is due to having only 2 pumps available on which to conduct testing. Initial testing of both pumps focused on baseline characterization of steady state and transient conditions across specific run speed setpoints conditions.

With respect to the second pump, testing focused primarily on permanently damaging subcomponents, inserting these various seeded fault subcomponents into the pump in place

of their no-fault component counterpart, and then conducting testing to determine if the fault could be detected by means of the pressure sensor. These tests focused first on seeding faults in the front bearing and then secondly by seeding a fault in the gear pump.

The ideal test plan would utilize a large sample size of actual pumps degraded over the course of real world operational service. We did not have access to such a sample set of pumps. Furthermore, the degrader analysis only identified the PT pump as a single monolithic component in terms of its responsibility as a contributor to overall fuel system failures. Due to data access limitations, the degrader analysis did not provide further details as to which subcomponent(s) within the PT pump were responsible for the pump's overall failure. Absent this information, the next best alternative was to simulate faulted pumps by seeding faults in the pump's subcomponents which anecdotally or hypothetically explained the pump's reported failure during fielded operation. The seeded faults were chosen to represent faults that were either reported by maintainers or potentially problematic given operating conditions. With this said, given the pumps are intended for use with JP8 fuel, and as such, the fuel system is required to be capable of operation with fuel containing impurities and particulate such as fine sand/dirt common in desert environments, two failure modes were chosen for test stand investigation: (1) bearing spalling and (2) accumulation of a particulate coating on the teeth of the gears within the gear pump sub-assembly. The following subsections will document the testing and analysis of: (1) simulated bearing spalling fault and, (2) simulated gear tooth particulate accumulation.

As indicated earlier in this report, the primary objective was to utilize the capability of the existing pressure sensor that is integrated into CMED variant Bradley platforms with the least complex and computationally intensive condition indicators. The rationale with respect to the evaluation progression was to start with the basic root mean square condition indicator and progress to more advanced statistical features if RMS is not effective for these faults and this application.

5.1 Bearing Fault Test Discussion

To summarize the motivation for the spalling fault tests, the rationale for investigating a simulated spall in the bearing raceway is based on the hypothesis that fine sand particles, which have infiltrated the fuel system, make their way into the bearing raceway. The repetitive impact of the roller elements passing over the particle(s) as they lay in the raceway results in pitting/spalling which increases in size over time. The subsequent imperfections in the surface of the raceway might potentially degrade the bearings performance and thereby the PT pumps performance. The purpose of the study is to investigate whether such a fault can be detected by the on-board pressure sensor located post-PT pump on the M2 CMED Bradley vehicle. This test initially set out to specifically investigate whether the bearing fault frequency known as the Ball Pass Frequency – Outer Race (BPFO) could be detected in the pressure spectrum. For completeness, the other three fault frequencies are referenced as follows: Ball Pass Frequency – Inner Race (BPFI), Ball Spin Frequency (BSF), Fundamental Train Frequency (FTF).

The analytical equations for these bearing fault frequencies displayed in subsequent plots are as follows according to (White, 1995):

$$BPFO = \frac{n}{2}\left(1 - \left(\frac{B_d}{P_d}\right)\cos\theta\right) RPM \quad (1)$$

$$BPFI = \frac{n}{2}\left(1 + \left(\frac{B_d}{P_d}\right)\cos\theta\right) RPM \quad (2)$$

$$BSF = \frac{P_d}{2B_d}\left(1 - \left(\frac{B_d}{P_d}\right)^2 (cos\theta)^2\right) RPM \quad (3)$$

$$FTF = \frac{1}{2}\left(1 - \left(\frac{B_d}{P_d}\right) cos\theta\right) RPM \quad (4)$$

The front bearing of the PT pump is a type NSK 6203. According to the manufacturer, the following specifications are:

Number of rolling elements (n):	8
Ball diameter (B_d):	6.746 mm
Pitch diameter of the bearing (P_d):	29 mm
Contact angle (θ):	0°

While the figures below include the fault frequencies in the subplot titles, we did not observe spectral peaks at these frequencies when analyzing the datasets.

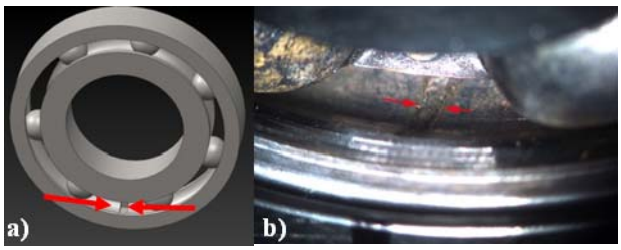

Figure 5. a) Electrolytically etched bearing outer raceway schematic format, b) Actual 0.030 inch etch

Electrolytic etching was selected instead of electric discharge machining (EDM) as the method of choice to create faults in the bearing raceway for this study because of the non-uniform spall edge it produced. This ad hoc technique was used specifically because of its ability to create non-uniform edges in the bearing raceway. No literature reference source was used as a precedent for this specific etching application. Electrolytic etching is essentially a controlled electrolytic corrosion process described in standard chemistry texts. Electrolytic corrosion is defined as a process of accelerated corrosion resulting

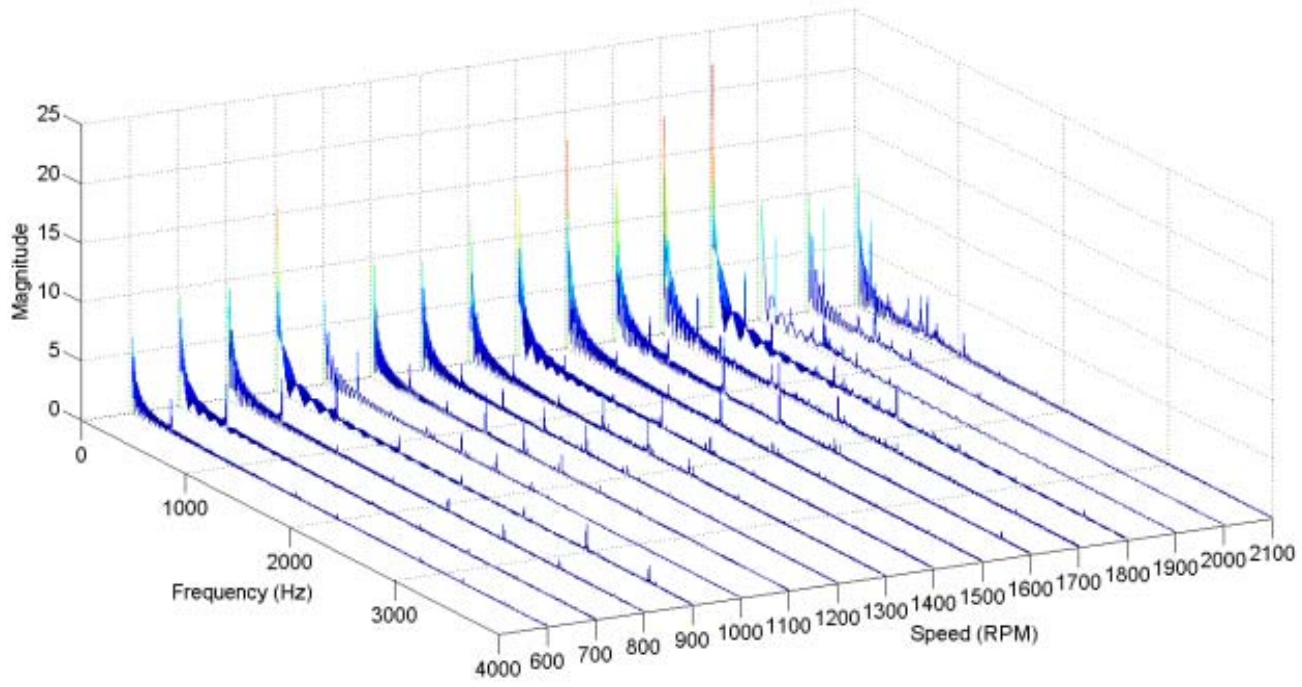

Figure 6. Representative waterfall plot depicting selected frequency domain spectrum of pressure transducer over the 600-2100 RPM speed setpoint conditions for a no-fault bearing test

from an electric current between two metals coupled in an electrolytic environment. (DTSFE, 2011). In this case the electrolytic environment was a saline solution.

The simulated spall testing, hereafter referred to as etched bearing or etched fault testing, was conducted with two bearings, each with a nominal etch width of 0.030 inch and 0.080 inch, respectively. Figure 5 depicts the faulted bearing in schematic form as well as a photo of the actual etched 0.030 inch faulted bearing. The chosen etch widths of 0.030 and 0.080 inch were dictated primarily by the precision limits of the equipment used to create the etch. A spall width of 0.080 inch is likely an over-exaggeration compared to a spall that may occur in a field environment. For initial investigation purposes our intent was to validate whether a bearing defect could be detected using the existing pressure transducer on the CMED platform. The test plan used to investigate whether the etched fault could be detected via the pressure transducers utilized 16 speed setpoint conditions ranging from 600-2100 RPM at wide open throttle along with four zero (0) RPM setpoint conditions used to characterize background ambient noise conditions when the pump main shaft was not rotating. Inspection of the background ambient noise data indicated potential electromagnetic interference due to the adjacent AC motor controller. While the methodology is valid, the statistical limitations due to pump sample size combined with the potential EMI limit the extent to which significance can be ascribed to the spectrum analysis discussed in the following sections.

Figure 6 shows the spectra for 16 run speed setpoint conditions. Similar waterfall plots showing all 16 speed setpoints were generated for the 0.030 inch and 0.080 inch etched bearing tests for both pressure transducer and accelerometer signals.

The next step of the analysis was to determine whether the pressure spectra contained visual/qualitative features indicating the presence of the etch in the bearing. To this end the initial approach taken was to overlay the spectra of the no-fault, 0.030 inch width and 0.080 inch width etched fault test at each speed setpoint and view the spectra across the 0-500 Hz operational bandwidth of the dynamic pressure transducer. Figure 7 illustrates a representative result of this overlay for one run speed setpoint condition at 1500 RPM. While there are distinguishable differences between the spectra, there was no specific distinguishable and repeatable feature observed across all run speed setpoints.

Recognizing the limits of visual inspection with respect to spectrum plots of this nature, an alternate approach was undertaken by which a root means square (RMS) calculation was computed for each no-fault, 0.030 inch and 0.080 inch fault spectrum across the entire spectrum range, respectively. Figure 8 depicts the results of this approach for four selected run speeds along with the RMS values for each fault condition displayed in the legend.

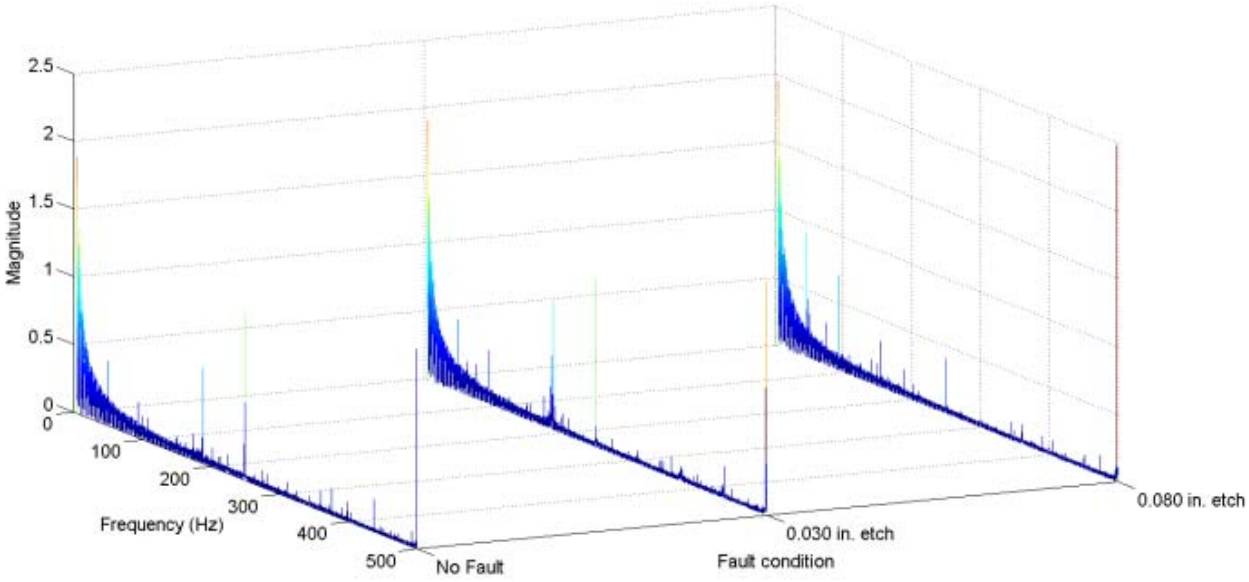

Figure 7. Waterfall comparison overlay of pressure spectrums for no-fault, 0.030 inch width and 0.080 inch width etched fault at nominal run speed 1500 RPM

It is observed that at three of these specific run speeds (600, 1000, and 1500 RPM), a simple RMS calculation produced condition indicator (CI) values that increased as etch width increased from no-fault through 0.030 inch to 0.080 inch width. Notice that the RMS values for the bottom plot (nominal run speed = 2000 RPM) did not support this trending correlation observed in the top three subplots. The bar graph in figure displays these RMS values in a graphic representation.

Note that at the 2000 RPM speed setpoint, the no-fault RMS value is greater than the 0.030 inch etch RMS value. This deviation from the trend was not an isolated outlier. The general RMS trending relationship observed between 600-2000 RPM across fault sizes was not repeatable for all speed setpoint conditions. In general, the RMS feature did not provide a consistent and highly sensitive condition indicator for bearing fault predictive detection.

Because the RMS based approach did not yield consistent results in terms of correlating RMS value to etch width for all speeds, we surmised that the potential reason for not detecting this correlation was perhaps due, at least in part, to the fact that utilizing the entire operational bandwidth of the pressure sensor may have been effectively masking RMS changes occurring within specific frequency ranges.

To address this point, we returned to the radial vibration data and observed the accelerometer's frequency spectrum at each run speed setpoint condition. The objective was to identify spectra peaks that; (1) remained constant across all run speed setpoint conditions, or (2) that predictably changed with respect to run speed, or (3) that somehow appeared to correlate with the width of the etched bearing fault. We would then use these peaks as a reference, or marker frequency about which we would isolate our RMS calculation of the pressure spectrum for the no-fault, 0.030 inch and 0.080 inch width etch fault tests. In general, using vibration spectrum peaks as a 'frequency marker' did not produce consistently repeatable RMS trend results.

This inconsistency in the RMS calculation even when using a vibration frequency marker as described above led us to investigate whether there were any frequencies, or frequency bands at which the RMS value of vibration spectrum increased with increasing etched fault width AND simultaneously, at these frequencies (or frequency bands), the RMS value of the pressure spectrum also increased with increasing etched fault width. Figure 10 shows a binary plot illustrating the results of this study for selected run speed setpoint conditions.

In long hand explanation, the algorithm plots either a 'TRUE' or 'FALSE' depending on whether the following condition is satisfied:
The plot is 'TRUE' or 'High', if:

(1) The vibration data is consistent in terms of the RMS value of the 0.080 inch etch spectrum is greater than the 0.030 inch etch spectrum;
(2) AND the RMS value for the 0.030 inch etch spectrum is in turn greater than the no fault spectrum;
(3) AND simultaneously the pressure data is consistent in terms of the RMS value of the 0.080 inch etch spectrum is greater than the 0.030 inch etch spectrum;

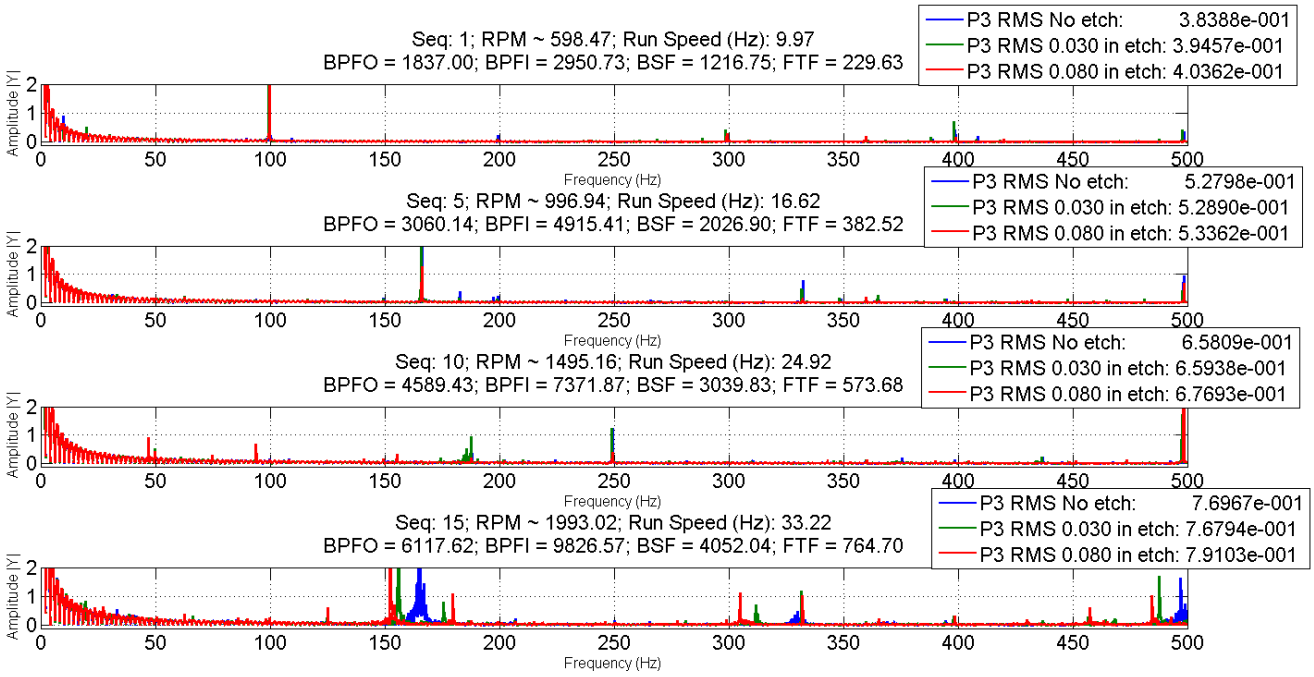

Figure 8. RMS calculations for no-fault, 0.030 inch width and 0.080 inch width etched fault spectrums for four selected run speed

(4) AND the RMS value for the 0.030 inch etch spectrum is in turn greater than the no fault spectrum.

Though the resolution is difficult to visually resolve across the entire 0-500 Hz bandwidth, there are frequency regions which the 'density' of TRUE conditions are relatively greater than for other regions. Even when comparing across multiple run speed setpoint conditions, there appears to be frequency bands that have corresponding TRUE vs. FALSE regions. However there does not appear to be a frequency band that is consistent across all run speed setpoint conditions.

Had a consistent frequency band been identified across all speeds, this frequency range would have been the focal point for developing a fault detection algorithm, specific to this bearing spalling fault.

To investigate the feasibility of implementing the RMS fault detection approach using the existing broad band vehicle sensor data, figure 11 distills in bar graph format the 0-500 Hz RMS results for the respective pressure spectra at multiple runs speeds. It should be noted that the results are not consistently repeatable across all run speeds.

Based on our limited data set, there appears to be speed regimes in which the RMS value increases with fault severity, as highlighted in figure 11. In general the RMS calculation has a number of limitations. For example it is common to observe significant variation in RMS values among pumps, engines and transmissions all of the same model type. It is therefore prudent that any condition monitoring algorithm incorporate multiple calculation approaches as a means of corroborating conclusions and minimizing false positive results.

There exist a number of techniques collectively referred to as statistical signal processing techniques or features that can also be applied. Four additional features were applied to the pressure signal data; Total Energy, Crest Factor,

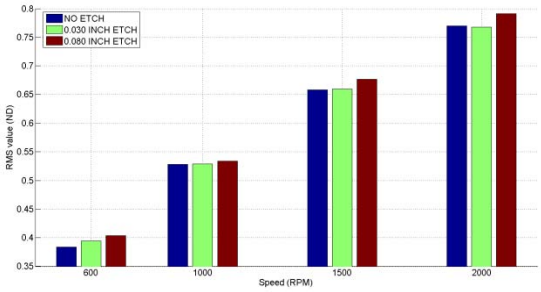

Figure 9. Bar graph plot of RMS calculations for no-fault, 0.030 inch width and 0.080 inch width etched fault spectrums at four selected run speeds

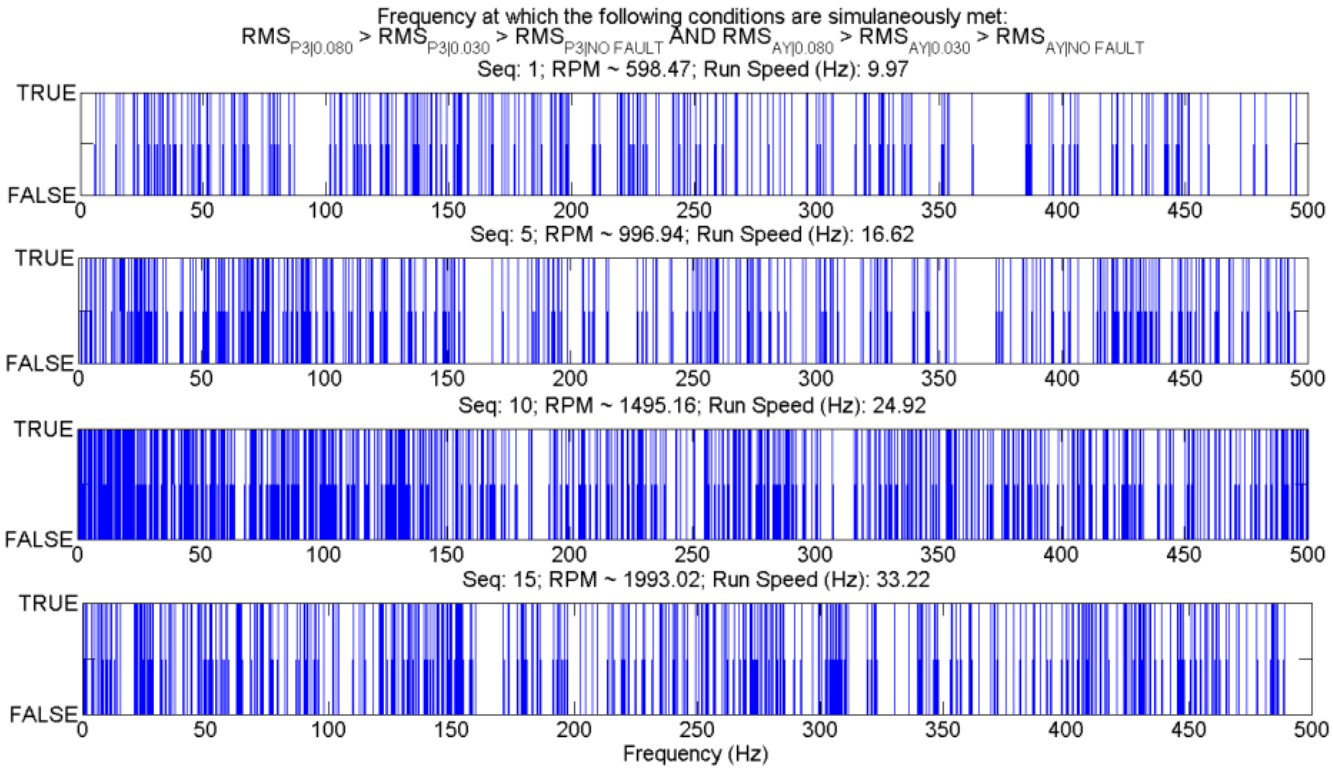

Figure 10. Identifying frequency bands for which the RMS value of the pressure spectrum increased with increasing etched fault width AND simultaneously at these frequencies the RMS value of the vibration spectrum also increased with increasing etched fault width

Kurtosis, and Kurtosis Interstitial Envelope. The results of the four methods also did not show consistent quantitative trends with respect to etch width. Representative of the inconsistency among the feature findings is figure 12. Figure 12 illustrates that the results of applying kurtosis did not provide the ability to predictively detect the various states of bearing condition consistently across every speed range, but it did provide a more sensitive predictive fault detection capability at one more of the speed setpoints relative to the RMS approach.

5.2 Etched Bearing Test Conclusion

The results of the of the bearing fault detection investigation indicated the RMS pressure spectrum from 0-500 Hz, as a condition indicator, has a low fault sensitivity and it is only effective for less than half of the speed setpoints that were tested. Specifically, the RMS calculation was not consistent across all 16 run speed setpoint conditions in the sense that the RMS values correlated with increasing etch width. Select individual speed setpoint conditions appeared to be consistent in terms of increasing RMS value vis-a-vis etch width but this was not consistent across all speeds. The kurtosis pressure spectrum from 0-500 Hz provided a predictive condition indicator with a slightly improved fault sensitivity as compared to the RMS feature. Though it is effective for more of the speed setpoints tested it is not effective for the entire speed range. In comparsion, the RMS accelerometer spectrum from 0-500 Hz provided a predictive condition indicator with the highest fault sensitivity as compared to the other features.

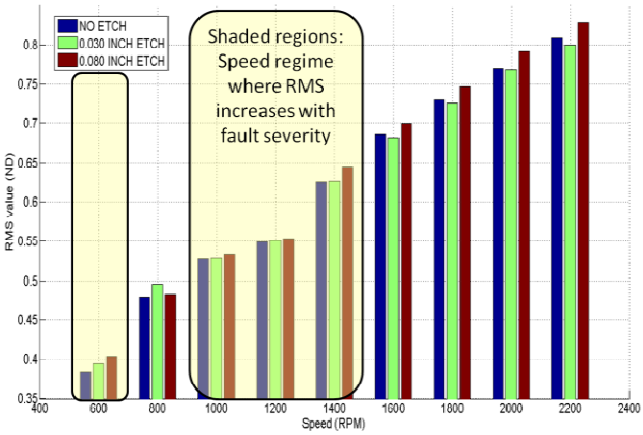

Figure 11. Bar graph summary of 0-500 Hz bandwidth RMS calculation for fuel pressure spectrum with bearing fault for nine run speed set point conditions

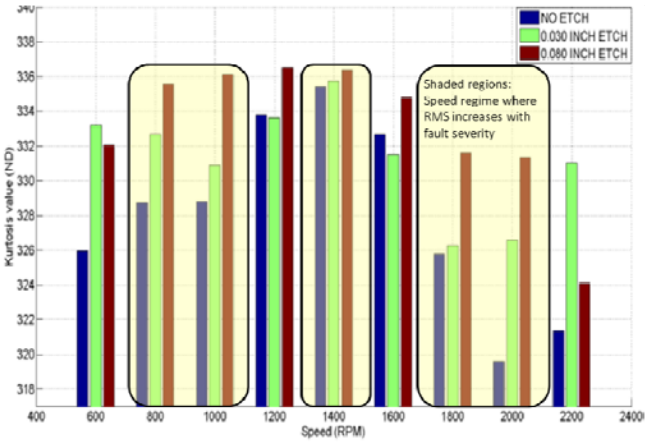

Figure 12. Bar graph summary of 0-500 Hz bandwidth Kurtosis calculation for fuel pressure spectrum with bearing fault for nine run speed set point conditions

5.3 Gear Fault Test Discussion

The aim of the gear fault testing was to investigate whether accumulation of particulate on the teeth of the gear pump sub-assembly could be detected by the downstream pressure transducer. As mentioned above, one individual maintainer/technician noted he was aware of at least one pump failing due to the pump shaft breaking because particulate accumulating on the gear teeth caused the gear pump to bind under load. Without reproducible evidence, this fault is difficult to conceptualize as a failure mode in practice. It is plausible that a larger piece of foreign-object-debris entered the gear pump and thus resulted in the shaft breaking due to the gears binding versus the failure resulting from the gradual accumulation of particulate on the gear teeth. Nevertheless, with this in mind, the following discussion documents our efforts to investigate this accumulation of particulate on the gear teeth as a potentially detectable failure mode.

Figure 13 shows the gear pump sub-assembly and the aluminum coating applied to one gear tooth for the simulated fault test. To re-iterate, the ideal test would utilize fielded gear pumps with particulate accumulated on the gear teeth or perhaps more likely in the gear's space width (teeth valleys). The gear fault testing incorporated only four run speed setpoint conditions compared to the 16 used for the subsequent bearing fault testing. The four run speeds were 600, 1300, 1700, 2100 RPM. These run speeds correspond to the four calibration setpoint conditions we obtained from the Cummins factory that calibrated our original PT pump.

The bar graph data in figure 14 summarizes the broadband RMS calculation of the fuel pressure spectrum for the no gear fault case (no coating) and the fault case (~0.001 inch coating) for the four run speed setpoint conditions.

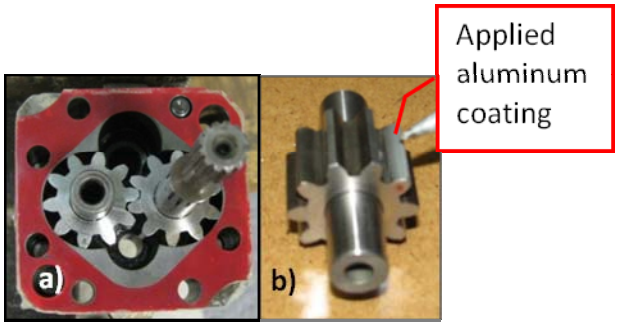

Figure 13. a) Gear pump sub-assembly, b) Metal coating applied to one gear tooth for simulated fault test

The data in figure 14 shows that this basic method does provide a low sensitivity condition indicator at the 1700 RPM and 2100 RPM pump speed setpoints but it does not provide an indication at 600 RPM and 1300 RPM. Based on these results the next step in the analysis was directed toward a narrowband frequency evaluation.

The spectrum characteristic we focused on was the distinct peak observed at 10X run speed or the 10th order as indicated by the yellow shaded box in figure 15. This frequency corresponds to the gear pump's Gear Mesh Frequency (GMF), which is equal to the shaft speed in Hertz multiplied by the number of teeth on the gear mounted on that same shaft.

With this stated, we continued the line of inquiry to examine whether a similarly consistent peak and RMS value would be detected in the pressure signal. Based on visual inspection, across this broad order range from 0 to 30 orders, there appeared to be two 'relatively' consistent indications of the gear fault in the pressure spectrum. The next step in the study focused on discrete frequency analysis as indicated by the two ordered frequencies marked in yellow as potential condition indicators in figure 15.

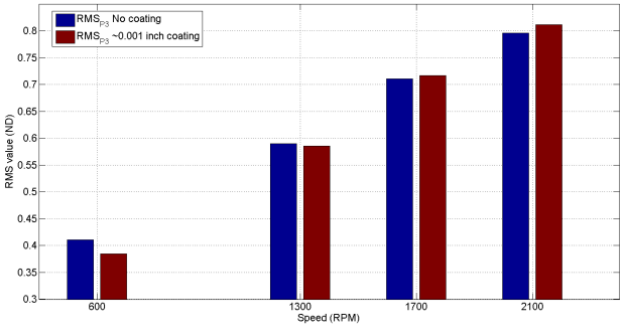

Figure 14. Bar graph summary of the broadband 0-500Hz RMS calculation of fuel pressure spectrum for the no gear fault case (no coating) and the fault case (~0.001 inch coating) for the four run speed set point conditions

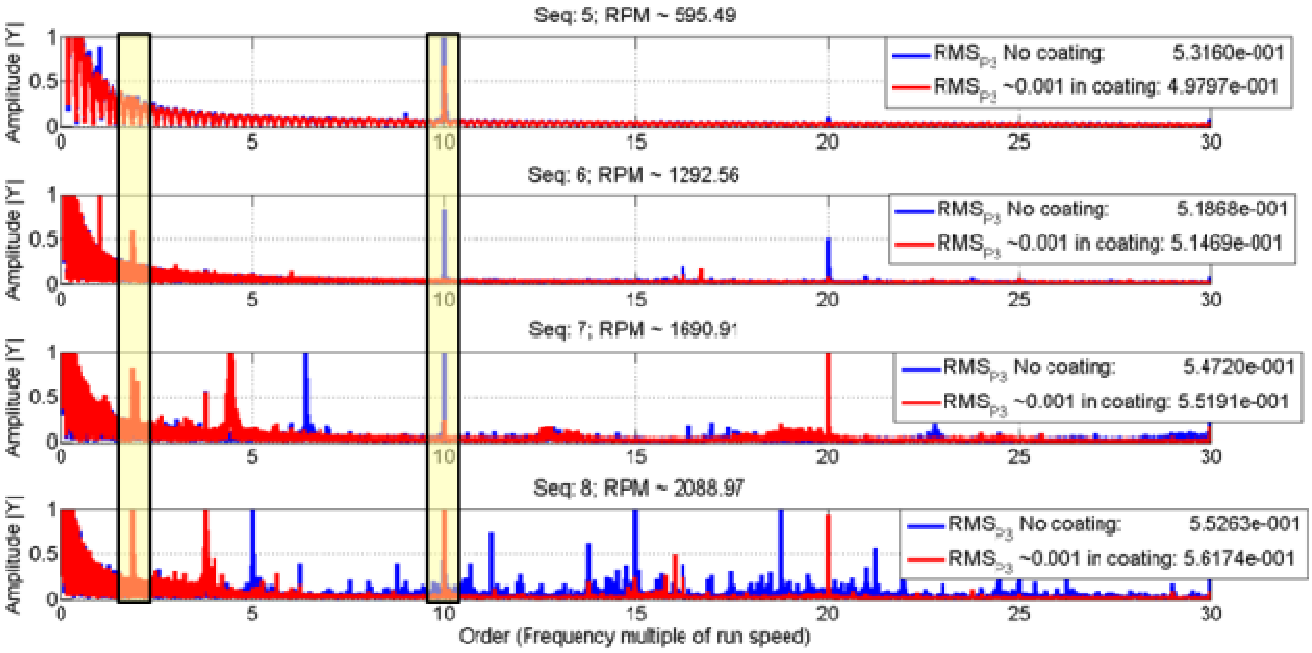

Figure 15. Fuel pressure frequency spectrum in the order domain with gear fault for the four run speed set point conditions

As stated above, because the 10th order frequency appears to be the most favorable ordered frequency marker, we narrowed our ordered frequency band over which we performed the RMS calculation to the 9th through 11th order range in order to determine whether a quantitative fault indicator may be more pronounced when only a specific band of the entire pressure spectrum is used for the calculation. However the RMS of the nominal 10th order frequency from the pressure sensor does not provide a positive correlation with the fault. It was therefore ruled out as a predictive condition indicator.

Based on visual inspection, the data indicates that there does appear to be a second discrete frequency in the pressure data that correlates to the seeded gear fault condition. This frequency is at approximately 1.8 orders as indicated in figure 15. The plot in figure 16 shows the positive correlation in the narrowband RMS calculation and the no fault versus seeded fault cases at the 1.8 order of run speed frequency. This finding suggests this discrete ordered frequency might potentially be useful as a predictive condition indicator. Pending further analysis using a statistically significant number of pumps, we emphasize two points: (1) There is no precedent or physical explanation providing the rationale to focus on the 1.8th order of run speed; This order was selected based on manual inspection of the spectrum. The objective was to identify orders at which the RMS results demonstrated a positive correlation with respect to presence of the gear tooth coating; (2) It is not yet confirmed whether the correlation at this run speed order is consistent for a larger sample set of pumps.

5.4 Gear Fault Test Conclusion

The results of the gear fault detection investigation are not decisive but did not rule out the potential for an effective predictive gear fault detection capability using the existing pressure sensor installed on the CMED variant Bradley.

The preliminary analysis conducted using the accelerometer data showed that the broadband (0-500 Hz) RMS vibration spectrum does not provide a predictive condition indicator. The discrete frequency analysis indicated that the 10th order, which is the gear mesh frequency for the gear pump, did not prove effective when utilized with the pressure sensor. The next step in the analysis led to an assessment of other effective discrete frequency indicators that could be used with the pressure sensor. It was determined that a discrete frequency at the 1.8th order could potentially be utilized as an

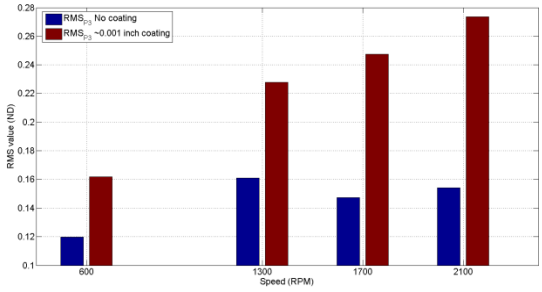

Figure 16. Bar graph summary of nominal 1.8th order RMS calculation of fuel pressure spectrum with gear fault for the four run speed set point conditions

effective predictive condition indicator for the gear fault case. The relationship between this frequency and the gear fault has not been determined at this point. Among other considerations, the effect of the pressure pulses generated by the fuel injectors requires study in order to rule out the potential it may possess to mask the characteristic spectral signature of this fault. Further testing would be conducted to validate this condition indicator.

6. CONCLUSION

This paper documents the test stand setup and analysis methodology used to investigate the feasibility of detecting seeded gear and bearing faults in a PT pump using an existing on-board M2 Bradley fuel pressure sensor with a dynamic bandwidth of 0-500 Hz. The results are not statistically valid, nor are the results consistent at all speed setpoint conditions. With this stated, there is limited evidence suggesting that it may be feasible to detect a 0.001 inch particulate accumulation on the gear pump teeth using narrowband RMS based quantification methods. Four additional statistical signal processing features yielded no more consistent results across the range of speed setpoints examined. The inconsistencies associated with run speed are not fully understood. Further study would enable confirmation as to whether structural frequencies associated with the pump or the test stand configuration may be contributing factors. The data processing employed in this study utilized a 100 kHz sampling rate to acquire the pressure signal and a one pulse per revolution tachometer signal for time synchronous averaging. Limitations to the data processing are dependent on the intended on or off-board end-use implementation. On/off-board implementation must address electro-magnetic interference and signal pre-conditioning considerations along with associated cable shielding, computer processing, data storage and user interface requirements. Given the relatively gradual lead up to PT pump failure given bearing and gear faults of this type, further study would investigate the cost effective feasibility of detecting such bearing and gear faults at idle speed using an at-platform maintenance-bay diagnostic software tool approach. While on-board detection at higher speeds may be feasible in theory, the additional cost of data acquisition, instrumentation and sensor/DAQ maintenance along with the complexity associated with noise in a field environment, may not justify maintenance and logistics costs.

ACKNOWLEDGEMENT

This work was supported by the NAVSEA Contract Number N00024-D-02-D-6604, Delivery Order Number 0356. The content of the information does not necessarily reflect the position or policy of NAVSEA, and no official endorsement should be inferred.

REFERENCES

Banks. J.C., Reichard, K.M., Hines, J.A., Brought, M.S. (2008). Platform Degrader Analysis for the Design and Development of Vehicle Health Management Systems. *IEEE Prognostics and Health Management (PHM) Conference*, October 6-9, Denver, CO. doi: 10.1109/PHM.2008.4711468

Cummins Component Shop Manual for Cummins PT Fuel Pump Rebuilding and Calibration Instructions (1980) Bulletin No. 3379084-02

Cummins Fuel Pump PT (type G) Calibration Values Bulletin No. 3379352-10

DTSFE (2011) Electrolytic corrosion http://www.dtsfe.com/faq/pdf/electolytic%20corrosion.pdf

Hines, J.H., Bennett, L., Ligetti, C., Banks, J.C., Nestler, S. (2009) Cost-Benefit Analysis Trade-Space Tool as a Design-Aid for the U.S. Army Vehicle Health Management System (VHMS) Program, *Prognostics and Health Management (PHM) Society 2009 Conference*, September 27-October 1, San Diego, CA.

Technical Manual 9-2350-294-20-1-1/3 (2006), Technical manual unit maintenance manual Fighting Vehicle, Infantry, M2A2 2350-01-248-7619, Department of the Army, December 1, 2006

White, D.G. (1995) *Introduction to Machine Vibration:* Bainbridge Island, WA, DLI Engineering Corp.: Part number 8569, version 1.76 (p. 110)

Jeffrey C. Banks is the Department Head of Complex Systems Engineering & Monitoring. His education includes a B.S.M.E. from Villanova University, Villanova, PA and a M.S. in Acoustics from The Pennsylvania State University, University Park, PA. He has 16+ years experience in applying advanced signal processing techniques, intelligent systems technology, and embedded diagnostics / prognostics tools to condition monitoring applications for the US Navy, US Marine Corps, US Army, NASA and Industry. His research engineer duties include developing machinery health management systems and diagnostic and prognostic technology for various DoD assets including the U.S. Marine Corps Expeditionary Fighting Vehicle (EFV), Light Armored Vehicle (LAV), AV-8B Harrier, U.S. Army Heavy Expanded Mobility Tactical Truck (HEMTT), Family of Medium tactical vehicles (FMTV) and U.S. Navy CVN class aircraft carriers. He has developed and delivered two short courses at all NASA facilities in the areas of Condition Based Maintenance (CBM) and Reliability Centered Maintenance (RCM). Additional responsibilities include conducting Failure Modes, Effects and Criticality Analysis (FMECA) for a variety of complex systems and platforms including aircraft engines and combat ground vehicles. He has also designed and developed diagnostic

instrumentation systems for machinery failure test beds and field data acquisition systems. He has first authored and published more than 18 papers in conference publications, and technical reports.
Before coming to Penn State ARL, he worked for the Mead Central Research Laboratory as a research engineer in the paper industry. He led over 100 diagnostic surveys at 9 separate paper manufacturing facilities and his primary functions were to troubleshoot machinery maintenance problems and process variability issues and develop unique predictive failure technology. He also developed and implemented vibration analysis surveys to evaluate resonance issues and condition of rotating elements and structural systems used in the paper industry.

J. Scott Pflumm is a research engineer at the Applied Research Laboratory. He received his B.S.M.E and M.S.M.E in Mechanical Engineering from Penn State University in 2002 and 2005 respectively. He served 3 years in the U.S. Army. His current work at ARL is in support of test and analysis of failure modes for ground vehicles at the sub-system and component level.